Icarus 221 (2012) 753–767

Contents lists available at SciVerse ScienceDirect

Icarus

journal homepage: www.elsevier.com/locate/icarus

The abundance, vertical distribution and origin of H_2O in Titan's atmosphere: Herschel observations and photochemical modelling ☆

Raphael Moreno [a,*], Emmanuel Lellouch [a], Luisa M. Lara [b], Helmut Feuchtgruber [c], Miriam Rengel [d], Paul Hartogh [d], Régis Courtin [a]

[a] LESIA–Observatoire de Paris, CNRS, Université Paris 06, Université Paris–Diderot, 5 Place Jules Janssen, 92195 Meudon, France
[b] Instituto de Astrofísica de Andalucía (CSIC), Granada, Spain
[c] Max-Planck-Institut für Extraterrestrische Physik, Garching, Germany
[d] Max-Planck Institut für Sonnensystemforschung, Katlenburg-Lindau, Germany

ARTICLE INFO

Article history:
Received 23 April 2012
Revised 7 September 2012
Accepted 7 September 2012
Available online 17 September 2012

Keywords:
Atmospheres, Composition
Photochemistry
Spectroscopy
Radio observations
Infrared observations

ABSTRACT

Disk-averaged observations of water vapor in Titan's atmosphere acquired with the Herschel satellite are reported. We use a combination of unresolved measurements of three H_2O rotational lines at 66.4, 75.4 and 108.0 μm with the PACS instrument, and spectrally-resolved observations of two other transitions at 557 GHz (538 μm) and 1097 GHz (273 μm) with the HIFI instrument, to infer the vertical profile of H_2O over the 100–450 km altitude range. Monitoring of the 66.4 μm line indicates no variation between Titan leading and trailing sides, nor variation over a ~1 year interval. Both the narrow (2–4 MHz) widths of the HIFI-observed lines, and the relative contrasts of the five H_2O lines indicate that the H_2O mole fraction strongly increases with altitude, with a best fit mole fraction of $q_0 = (2.3 \pm 0.6) \times 10^{-11}$ at a pressure $p = 12.1$ mbar, a slope $-d(\ln q)/d(\ln p) = 0.49 \pm 0.07$, and a H_2O column density of $(1.2+/-0.2) \times 10^{14}$ cm^{-2}. This H_2O profile also matches the original ISO observations of Titan H_2O. Water vertical profiles previously proposed on the basis of 1-D photochemical models are too water-rich, and none of them have the adequate slope; in particular, the water profiles of Lara et al. (Lara, L.M., Lellouch, E., López-Moreno, J.J., Rodrigo, R. [1996]. J. Geophys. Res. E 101, 23261–23283) and Hörst et al. (Hörst, S.M., Vuitton, V., Yelle, R.V. [2008]. J. Geophys. Res. E 113, E10006) are too steep and too shallow, respectively, in the lower stratosphere. Photochemical models of oxygen species in Titan's atmosphere are reconsidered, updating the Lara et al. model for oxygen chemistry, and adjusting the eddy diffusion coefficient in order to match both our H_2O observations and the C_2H_6 and C_2H_2 vertical profiles determined from Cassini/CIRS. We find that the H_2O profile can be reproduced by invoking a OH/H_2O influx of $(2.7–3.4) \times 10^5$ mol cm^{-2} s^{-1}, referred to the surface. This is essentially one order of magnitude lower than invoked by previous modellers, and also a factor of ~10 less than required to match the observed CO_2 mole fraction. As H_2O has a more shorter atmospheric lifetime than CO_2 (~9 years vs ~450 years), we suggest that this reflects a temporal change in the oxygen influx into Titan, that could be currently much smaller than averaged over the past centuries. Both interplanetary dust particles and Enceladus' activity appear to provide sufficient supply for the current Titan H_2O. We tentatively favor the latter source as potentially more prone to time variability.

© 2012 Elsevier Inc. All rights reserved.

1. Introduction

The detection of water vapor in the stratosphere of all four Giant Planets and Titan from Infrared Space Observatory (ISO) observations in 1996–1997 (Feuchtgruber et al., 1997; Coustenis et al., 1998; Lellouch et al., 2002) provided the long-awaited ultimate proof of the existence of an external supply of oxygen to these atmospheres. In the case of Titan, this expectation held for over 30 years, since the discovery of CO_2 by Voyager (Samuelson et al., 1981), as CO_2 can be efficiently formed from the reaction between OH, produced from the photolysis of H_2O, and carbon monoxide, that was discovered shortly after Lutz et al. (1983). As for all outer planets, the main question is the origin of this external flux. Three potential sources have been identified (see e.g. Feuchtgruber et al., 1997; Moses et al., 2000): (i) micrometeorite ablation (ii) cometary impacts (iii) local (satellite, ring) sources. Cometary impacts (in the outer planets) have been invoked as sources of CO in Jupiter, Neptune and Saturn (Bézard et al., 2002;

☆ *Herschel* is an ESA space observatory with science instruments provided by European-led Principal Investigator consortia and with important participation from NASA.

* Corresponding author.
E-mail address: raphael.moreno@obspm.fr (R. Moreno).

0019-1035/$ - see front matter © 2012 Elsevier Inc. All rights reserved.
http://dx.doi.org/10.1016/j.icarus.2012.09.006

Lellouch et al., 2005; Hesman et al., 2007; Cavalié et al., 2010) and H_2O in Jupiter (Lellouch et al., 2002). However, this might not be a promising source of volatiles for Titan given the scarcity of primordial noble gases in its atmosphere (Bézard, 2009). Up to now, disentangling between the other two sources has proven difficult (Coustenis et al., 1998; Moses et al., 2000).

Except in the case of spatially-resolved observations, which can in principle reveal horizontal variations related to the nature of the source, distinguishing between different sources usually requires translating the measured water columns into an input flux, which can then be compared to expectations from the various possible sources. This step involves the use of a photochemical model, including chemistry and transport. Coupled descriptions of atmospheric chemistry and general circulation are still in their infancy for Titan. Hence, models addressing Titan's oxygen chemistry (Yung et al., 1984; Toublanc et al., 1995; Lara et al., 1996; Wilson and Atreya, 2004; Hörst et al., 2008; Krasnopolsky, 2009) are so far 1-D models in which vertical transport is parameterized by an eddy diffusion coefficient profile, usually constrained by the vertical distribution of species with sufficiently well known chemistry (e.g. simple hydrocarbons). In a broad sense, the above models concluded to large H_2O fluxes, encompassing the $(0.6–9)\times10^6\,cm^{-2}\,s^{-1}$ range (see Strobel et al. (2010) for a review of the recent work). Still, the original ISO detection did not provide any information on its vertical profile, as the observed lines could be fit equally from a vertically constant H_2O abundance (above its condensation level in the lower stratosphere) or by rescaling predictions of one of the above models (Lara et al., 1996), resulting in a mole fraction profile with a steep vertical slope. H_2O measurements from Cassini turned out to be difficult. In the upper atmosphere, the Cassini Ion Neutral Mass Spectrometer (INMS) only reported upper limits of H_2O at ~1100 km (Vuitton et al., 2007; Cui et al., 2009). In the stratosphere, a positive detection of water lines at 40–60 μm from the Composite Infrared Spectrometer (CIRS) had to await the improvement of the instrument calibration pipeline. In a recent study, Cottini et al. (2012) analyzed large averages of Cassini/CIRS spectra in limb and nadir geometry and demonstrated that the H_2O mole fraction does increase with altitude from 125 to 225 km, as expected for a species with a high-altitude source and a low-level photolysis and condensation sink.

With its three spectrometers, the Herschel observatory (Pilbratt et al., 2010) is well equipped to observe Titan's water. The Spectral and Photometric Imaging REceiver (SPIRE) instrument (Griffin et al., 2010) does not have sufficient spectral resolution to detect the faint water lines expected over 196–671 μm (Courtin et al., 2011). Much stronger lines, comparable to those seen by ISO around 40 μm, fall in the wavelength range 55–180 μm covered by the Photodetector Array Camera and Spectrometer (PACS) instrument (Poglitsch et al., 2010) at suitable spectral resolution. Furthermore, the $\sim10^6$–10^7 resolving power afforded by the Heterodyne Instrument for the Far-Infrared (HIFI, de Graauw et al., 2010) makes it ideally suited to the observation of narrow stratospheric emission lines. We report here on combined PACS and HIFI observations of Titan water – conducted in the framework of the Herschel Key Programme "Water and related chemistry in the Solar System" (Hartogh et al., 2009) – from which we determine the H_2O abundance and its vertical distribution in Titan's atmosphere. Observations are described in Section 2, and their modelling in Section 2. Results are then interpreted with the help of a photochemical model to provide updated estimates of the external flux of water into Titan (Section 4). Results are finally discussed in terms of the possible nature of this supply (Section 5).

2. Observations

2.1. PACS observations

Disk-averaged observations of several far-infrared lines of water on Titan's atmosphere have been obtained using the Herschel/PACS spectrometer in 2010 and 2011. Observations dates are listed in Table 1. The $H_2O(2_{21}–1_{10})$, $H_2O(3_{21}–2_{12})$ and $H_2O(3_{30}–2_{21})$ transitions, at 108.1, 75.4 and 66.4 μm, respectively, were measured. The standard chopped–nodded PACS Line Spectroscopy mode (Poglitsch et al., 2010) with small chopper throw (±30″) has been used for all measurements. To avoid any spectral contamination from Saturn, all observations have been executed close to maximum elongation. In particular, the 66.4 μm line was observed four times, sampling both the leading and trailing sides of Titan.

The data reduction started from the Level 0 products generated according to the descriptions in Poglitsch et al. (2010). Level 1 processing has been run within HIPE 8.0 through all standard steps for chop–nod observations. All further processing (flatfielding, outlier removal and rebinning) has been carried out with standard Interactive Data Language (IDL) tools. The final bin size has been chosen close to Nyquist sampling at the observed wavelengths. The wavelength scale has been corrected to rest frame by removing the Herschel–Titan Doppler velocity shift. The double differential signal derivation from the chop–nod pattern is robust against introducing erroneous signal offsets. However, the absolute flux calibration is significantly affected by spacecraft pointing offsets, which can produce noticeable effects for a mispointing as low as 1.5″, with potentially different contributions at the individual nod positions. Dividing the spectra by the continuum in the vicinity of the observed lines, these and in fact also all other contributions for absolute flux calibration uncertainties cancel out. Thus, only the actual signal-to-noise ratio (SNR) in the measurements remains as main contributor for calibration uncertainties. Therefore, in the analysis of our spectra, the continuum divided approach has been preferred. Titan is an ideal point source as seen by the PACS spectrometer and consequently the data presented here only originate from the central spatial pixel (9.4″ × 9.4″) of the 5 × 5 integral field spectrometer. The inspection of the measured signal distribution on the entire 5 × 5 field of view shows that any potential contribution from Saturn at the central spatial pixel is well below 0.5 Jy (i.e. <1% of the peak flux) and can be neglected.

The various PACS spectra (108.1 μm, 75.4 μm, and the four observations at 66.4 μm) are shown in Fig. 1. For the June 2010 observations, the SNR at 108, 75 and 66 μm, are about 5, 13 and 10, respectively. No significant intensity variation (within 10%) of the 66.4 μm line is seen on the trailing side from June 2010 to

Table 1
Summary of PACS observations.

UT start date (yyyy mm dd.ddd)	Line (μm)	Sub-observer longitude (°)
2010 06 22.955	75.38[a], 108.07[a]	283
2010 06 22.992	66.43[b]	284
2010 12 15.363	66.43[b]	267
2010 12 23.973	66.43[b]	101
2011 07 09.588	66.43[b]	247

Notes: Observations by standard chop–nod PACS Line Spectroscopy. The spectral resolution for point sources is 0.020, 0.040 and 0.113 μm at 66.4, 75.4 and 108.1 μm, respectively.

[a] 3 Scan repetitions for a total time of 1160 s.

[b] 2 Scan repetitions for a total time of 800 s.

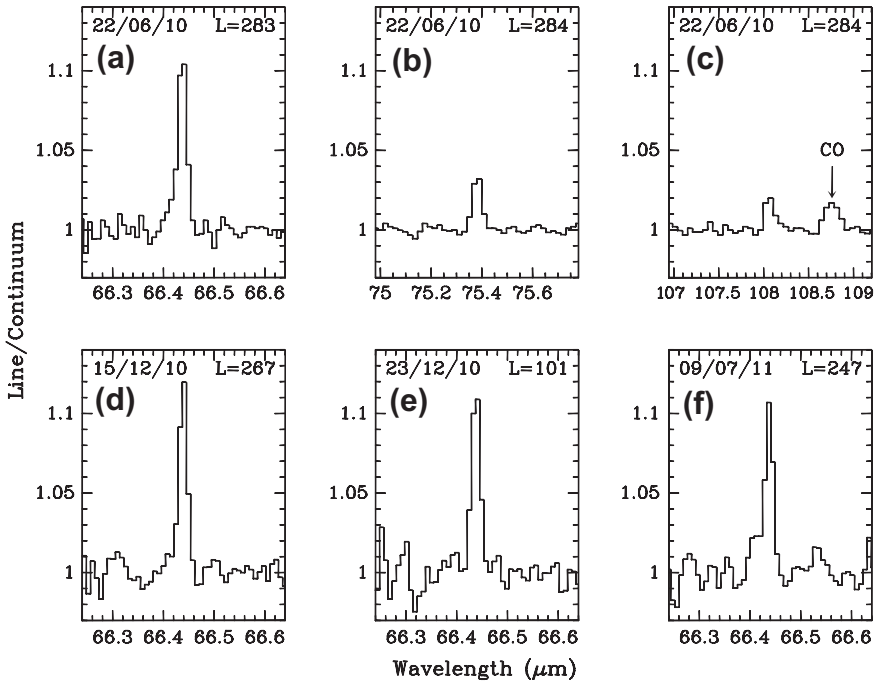

Fig. 1. PACS observations of the water lines at 66, 75 and 108 μm. The spectral resolution is 0.113, 0.040 and 0.020 μm, respectively. Observations dates (dd/mm/yy) and sub-observer longitude (L) are indicated. The intensity scale is expressed in line/continuum ratio.

December 2010 and July 2011 (Fig. 1a, d, and f), nor between the leading and trailing sides observations in December 2010 (Fig. 1d and e). This suggests a constant–with–longitude water abundance, stable on a ∼1 year timescale.

2.2. HIFI observations

Observations of Titan with the HIFI receiver in band 1a and 4b, using two H and V orthogonal polarizations, were obtained in June 2010, December 2010, and June 2011. Two water lines, namely $H_2O(1_{10}–1_{01})$ at 556.936 GHz (538 μm) and $H_2O(3_{12}–3_{03})$ at 1097.364 GHz (273 μm), were targeted. Typical integration times were 4 h. A summary of the HIFI observations is given in Table 2.

The detailed HIFI instrument performances can be found in Roelfsema et al. (2012). The spectral resolution of HIFI is 1.1 MHz (Wide Band Spectrometer – WBS) and 0.25 MHz (High Resolution Spectrometer – HRS). At 557 and 1097 GHz, respectively, the beam size (HPBW) is equal to 38.1″ and 19.3 ″, much larger than Titan's apparent diameter (∼0.75″), and therefore – like for PACS – all our measurements are disk-averaged.

The receiver beam efficiency (B_{eff}) are equal to 0.76 and 0.74, at 557 and 1097 GHz, respectively. The forward efficiency (F_{eff}) is equal to 0.96 at both frequencies.

These efficiencies are needed to convert the spectra measured in antenna temperature (T_a) to main beam temperature (T_{mb}) (and ultimately to Rayleigh–Jeans temperature – T_{RJ} – for comparison with models; see Section 3.1).

To avoid contamination from Saturn, the Titan observations were scheduled near its maximum elongation. The first measurement recorded at 557 GHz (June 2010) was performed using the position switch observing mode (PSw), with a reference position at +2′ north of Titan. This measurement revealed that the H_2O line appeared as a very narrow emission, with a full width at half-maximum (FWHM) of about 2 MHz. Thus, in order to improve the SNR, the standard frequency switching observing mode (FSw) was adopted for the other two observations (December 2010 and July 2011). Data reduction was carried out using the Herschel data reduction software (HIPE, Ott, 2010) which allows to calibrate and average each dataset, and to correct for the Titan–Herschel velocity. Additional baseline removal was then applied.

Due to SNR limitations, we focused on the 1.1 MHz resolution spectra. The 557 GHz was detected with a SNR ∼3–4 in each observation, yielding a SNR of ∼6 for the combined data. The SNR on the single 1097 GHz observation is 5. The final spectra are presented in Fig. 2. This is the first time that spectrally resolved water lines are measured in Titan's atmosphere.

Table 2
Summary of HIFI observations.

UT start date (yyyy mm dd.ddd)	Line (GHz)	Obs. mode	Δ (AU)	θ (″)
2010 06 14.822	556.936	PSw	9.390	0.756
2010 12 31.321	556.936	FSw	9.661	0.735
2011 07 02.265	1097.365	FSw	9.571	0.742

Notes: Observations were conducted using the standard position switching (PSw) and frequency switching (FSw) observing modes. The typical integration time was 4 h. Δ is the distance between Titan and Herschel. θ is the apparent diameter corresponding to Titan's surface.

3. Modelling

3.1. Radiative transfer model

The HIFI and PACS water spectra were analyzed using a line-by-line radiative transfer code with spherical geometry (Moreno et al., 2011, and references therein). This code takes into account the collision-induced absorption (CIA) due to N_2–N_2, N_2–CH_4, and CH_4–CH_4 pairs (Borysow and Frommhold, 1986, 1987; Borysow and Tang, 1993), as well as haze opacities (see below). The H_2O line parameters are taken from the JPL catalog (Pickett et al., 1998).

For the H_2O–N_2 pressure-broadening coefficients (γ_0), we used a value of $\gamma_0 = 0.115\ cm^{-1}\ bar^{-1}$, for the two HIFI water lines (Golubiatnikov et al., 2008; Seta et al., 2008; Cazzoli et al., 2009) at a reference temperature of 300 K and with a temperature

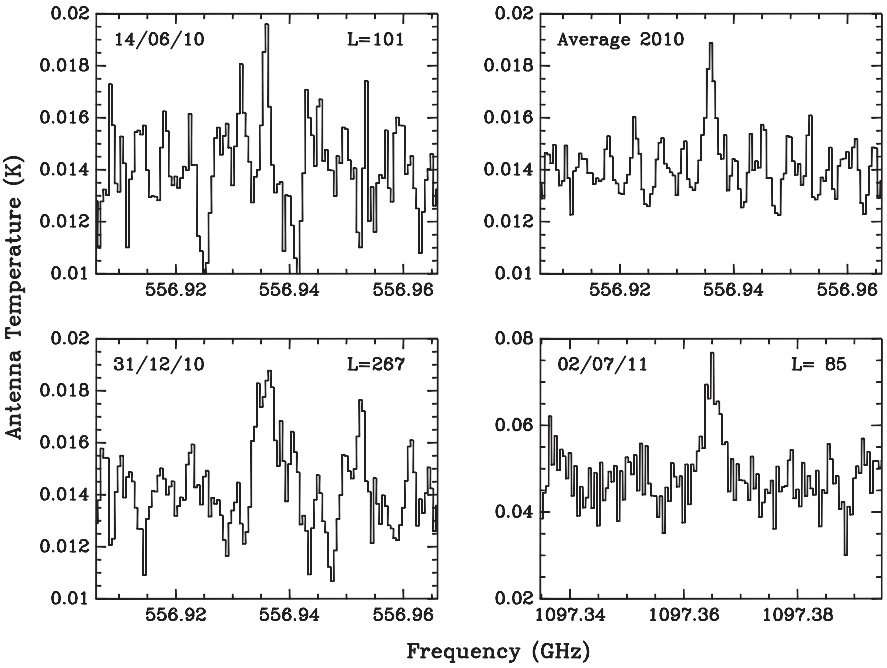

Fig. 2. HIFI spectra measured at 557 and 1097 GHz and expressed in antenna temperature (K). The spectral resolution is 1.1 MHz. Observations dates (dd/mm/yy) and sub-observer longitudes (L) are indicated. The top right box shows the average of the 2010 June and December 557 GHz observations.

dependency exponent $n = 0.76$. For the PACS lines, we used $\gamma_0 = 0.105\ \mathrm{cm^{-1}\ bar^{-1}}$ (Lynch et al., 1998).

For Titan's atmosphere thermal profile – P(T) – we used a combination of the Huygens Atmospheric Structure Instrument (HASI) profile (Fulchignoni et al., 2005) below 140 km, and Cassini/CIRS stratospheric temperatures (Vinatier et al., 2010) above 140 km, which were disk-averaged as described in Moreno et al. (2011). Model results indicate that inferences on the water abundance and distribution are relatively insensitive to temperature uncertainties. This results from the fact that the water lines are essentially optically thin: for the two HIFI lines, H_2O line opacities at the central frequency (integrated over the viewing geometry) are between 0.05 and 0.08, while those of PACS are in the range of 0.26–0.46. As a matter of fact, we have checked that even a large decrease of the stratopause temperature by 8% (i.e. almost 15 K), does not change significantly the computed line contrasts (< few %). With our best fit solution profile (shown in Fig. 3), the HIFI lines at 557 and 1097 GHz typically probe altitudes between 200 and 450 km, while the PACS lines at 108, 75, and 66 μm probe altitudes just above the water condensation level, i.e. between about 93 and 150 km (see Fig. 3). Thanks to the difference in altitude between the levels probed by the two instruments, we have the possibility of retrieving the water vertical profile.

In addition to CIA, haze is an important contributor to continuum emission originating from Titan's limb in the far-infrared (50–500 $\mathrm{cm^{-1}}$, i.e. 20–200 μm, Samuelson and Mayo, 1991; de Kok et al., 2007; Anderson and Samuelson, 2011). An accurate modelling of our observations therefore requires including haze emission, especially for the analysis of the PACS data (60–150 μm) in terms of line/continuum ratio. We used results on the haze vertical distribution and spectral dependence constrained from CIRS measurements (Anderson and Samuelson, 2011). We found that including the haze emission leads to an increase of the disk-averaged continuum emission by 1%, 2.5% and 6% respectively at 150, 100 and 60 μm. This is thus a small effect, but despite its small magnitude, this component is required for an optimum match of the PACS observations of water. Finally, synthetic spectra were calculated with a sufficient sampling to resolve the gaussian core of the H_2O lines before convolution to the appropriate instrumental spectral response functions.

3.2. Semi-empirical water profiles

A simple, vertically-uniform water mole fraction above a given level cannot simultaneously fit the HIFI and PACS observations. The narrow width of the lines observed by HIFI indicates that the bulk of water is restricted to altitudes above 300 km (similarly to HNC, see Moreno et al., 2011). An uniform mole fraction of $(0.8 \pm 0.2) \times 10^{-9}$ would then be needed above 300 km. However, fitting the PACS observations with such a profile would then require an inconsistent H_2O mole fraction of $(8 \pm 2) \times 10^{-9}$ (i.e. one order of magnitude larger than for HIFI).

As discussed in Section 4, a water profile increasing with altitude is expected as water has a high-altitude source and a low-altitude sink (photolysis and condensation). Therefore, we investigated semi-empirical profiles in which the H_2O mole fraction (q) increases with altitude as $q = q_0 \times (p_0/p)^n$, where p_0 is a reference pressure level, at which the H_2O mole fraction is q_0, and n the power law index.

Many simulations (>100) have been performed, exploring the q_0, n parameter space (q_0: (0.5–6) $\times 10^{-11}$, n: 0–1) and choosing p_0 near the condensation level. Based on χ^2 analysis, the best-fit solution of the ensemble of HIFI and PACS observations corresponds to $p_0 = 12.1$ mb (i.e. 93 km), $q_0 = 2.3 \times 10^{-11}$ and $n = 0.49$ (model S_a), which yield a water mole fraction of 6.4×10^{-10} at a pressure level of 0.0137 mbar (i.e. 400 km). In essence, this slope is required to match the relative contrast of the HIFI and PACS lines (illustrated in Fig. 4 for the 75.4 μm and 557 GHz lines). Limiting models S_b and S_c (fits within about 1σ of observations) correspond to $q_0 = 1.7 \times 10^{-11}$ and $n = 0.56$ (model S_b), and $q_0 = 2.9 \times 10^{-11}$ and $n = 0.42$ (model S_c). Note how the profile with the maximum acceptable slope (S_c) tends to overestimate the relative HIFI/PACS line contrast, and vice versa for profile S_b which has the minimum slope. The vertical distributions of models S_a, S_b and S_c are presented in Fig. 3. The vertically integrated column density for model S_a, and its uncertainty computed from models S_b and S_c, is

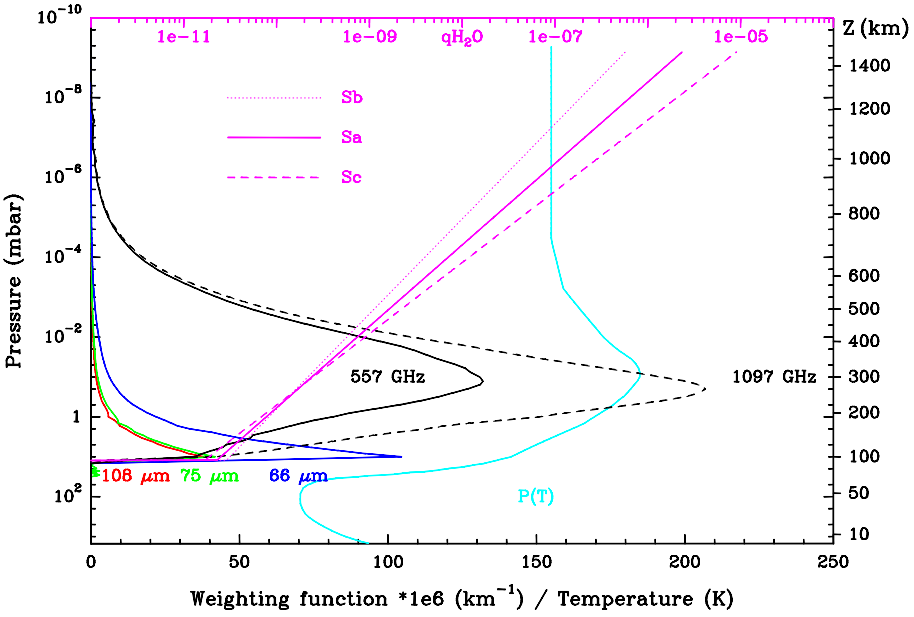

Fig. 3. Weighting functions for the various water lines observed with PACS and HIFI (averaged over our viewing geometry, and with the continuum contribution subtracted), computed with the best fit semi-empirical water vertical distribution (model S_a, see Section 3.2) of the H_2O mole fraction (qH_2O, top scale). Envelope profiles S_b and S_c are also plotted. The temperature profile used in our modelling is also shown (P (T), bottom scale).

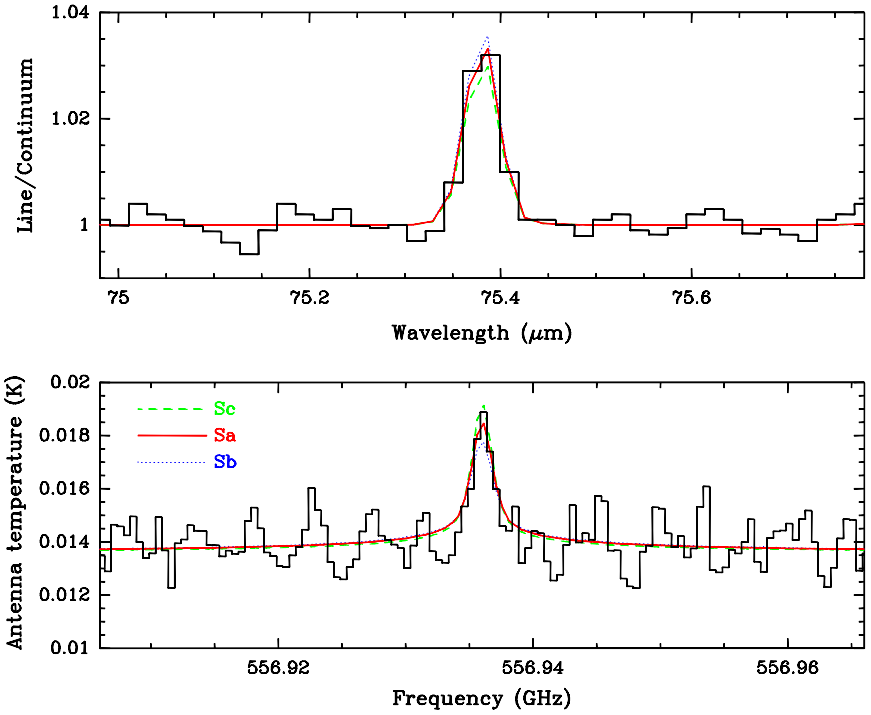

Fig. 4. Synthetic spectra computed with the models S_a, S_b and S_c of water mole fraction (see Fig. 3), compared to the PACS observation of the 75 μm line (top), and the HIFI averaged 557 GHz line (bottom).

$(1.2 \pm 0.2) \times 10^{14}$ cm^{-2}. As shown in Fig. 5, model S_a permits a good match to all our Herschel PACS + HIFI observations. As we will show later, this profile also provides a good agreement with the ISO observations of (Coustenis et al., 1998). Model S_a is also shown in Fig. 6 in the context of other physically-based models of the H_2O distribution (see below).

3.3. Test of previously proposed physical models

We also tested several models previously proposed on the basis of photochemical modelling. We considered especially (i) the model adopted by Coustenis et al. (1998) to match the ISO observations (i.e. the photochemical model of Lara et al. (1996), rescaled by a

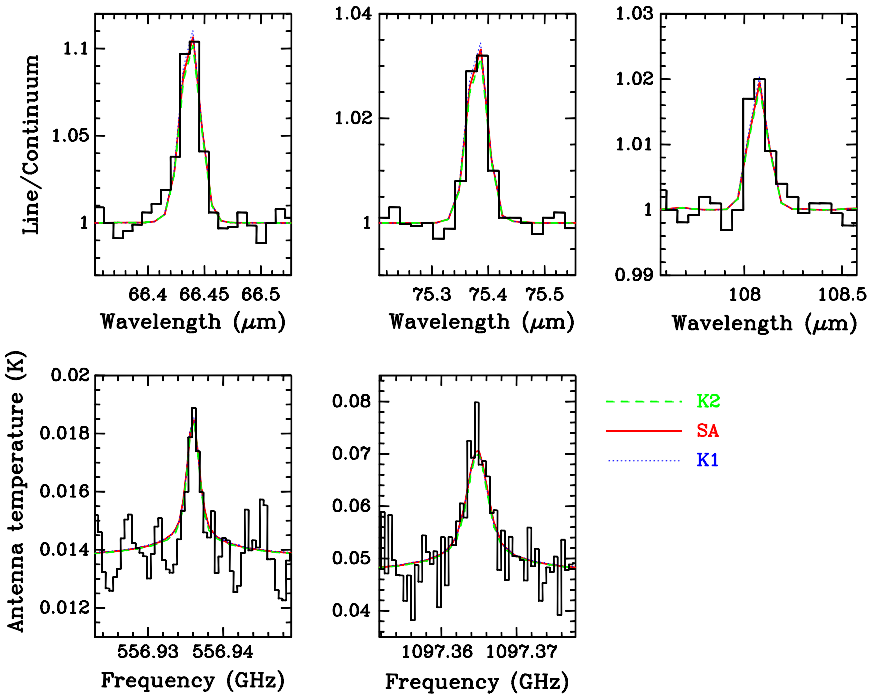

Fig. 5. Synthetic spectra computed with semi-empirical (S_a) profiles of the water mole fraction, and two photochemical models (K_1 and K_2, see Section 4), compared with the ensemble of PACS and HIFI observations. The associated mixing ratio profiles are shown in Fig. 6.

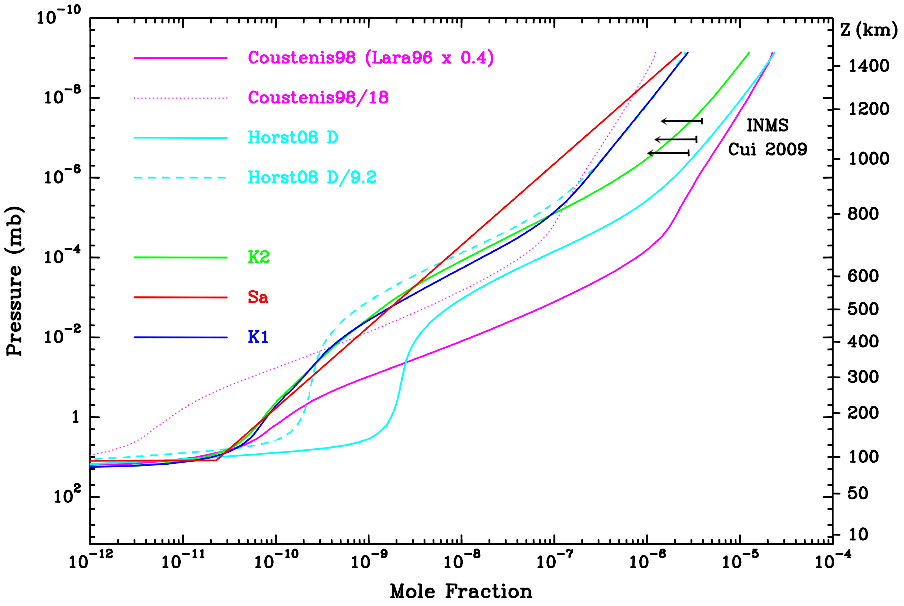

Fig. 6. Several vertical profiles of H_2O. Best fit semi-empirical profile (S_a); previously proposed models from Coustenis et al. (1998) and Hörst et al. (2008), and rescaled versions of these; and new photochemical profiles from this work (K_1 and K_2, see Section 4). The arrows indicate the 3-σ upper limits from INMS (Cui et al., 2009).

factor 0.4) (ii) the more recent models of Hörst et al. (2008), and in particular their preferred "model D" (see below Section 4 for details on these profiles). Focussing on the 75.4 μm (PACS) and 557 GHz (HIFI) lines, Fig. 7 demonstrates that none of these profiles provides an adequate match of the PACS + HIFI line dataset, as we will now discuss.

As it is obvious from Fig. 7, both the Coustenis et al. (1998) model and the Hörst et al. (2008) model D strongly overestimate the observed contrasts, for both lines. The same is true even of Hörst et al. (2008) model A, which follows the shape of their model D but has smaller water vapor mole fractions due to a lower influx rate. Matching the contrast of the 557 GHz line would require dividing the Coustenis et al. (1998) profile by a factor 18, and the Hörst et al. (2008) model D by a factor 9.2. In the latter case (model D/9.2), however, the model produces unobserved linewings; furthermore the PACS lines would then be somewhat overestimated. Both aspects indicate that the Hörst et al. (2008) models are too "water-rich" in the lower stratosphere ($z \leqslant 400$ km), producing too much emission in the spectrally-resolved Lorentz wings and – if rescaled to the HIFI line contrast – too much unresolved emission in the PACS lines. The opposite situation is encountered for profiles following the shape calculated by Lara et al. (1996): when

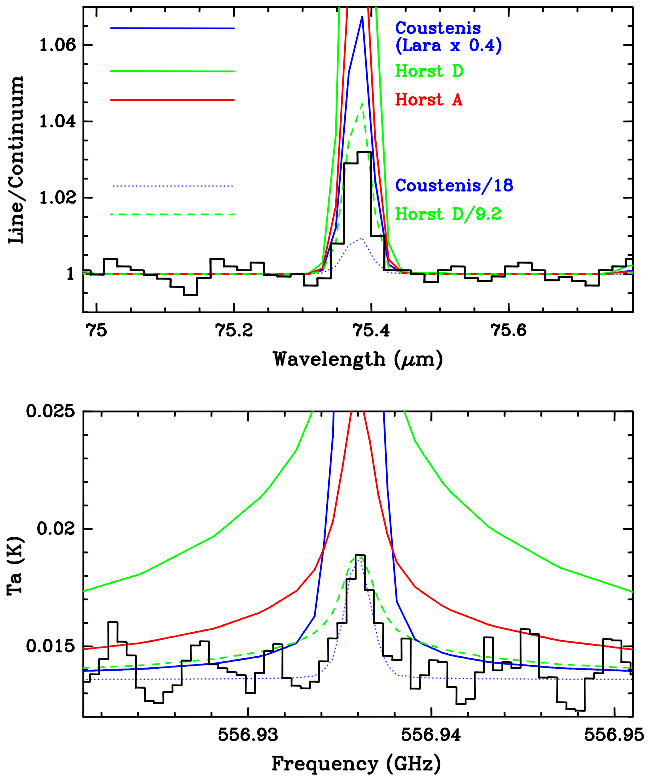

Fig. 7. Synthetic spectra computed considering several previously proposed H_2O profiles: Coustenis et al. (1998), Hörst et al. (2008) (model D and model A), and rescaled versions of these models. None of the models provides an adequate simultaneous match to the PACS observation at 75 μm (top) and HIFI at 557 GHz (bottom).

the Coustenis et al., 1998 profile is divided by 18, a good fit is achieved on the HIFI line, but the PACS line is then underestimated, indicating that this family of profiles does not contain enough water at the lower altitudes (93–150 km) compared with its abundance at 300–450 km. Therefore, we conclude that the previous photochemical models need revision, not only in the calculated absolute amount of water, but also in its vertical distribution.

4. Photochemical models

Because it is a species subject to photolytic, chemical and condensation losses, water vapor present in Titan's stratosphere must be of external origin. Knowledge about the existence of an external supply of oxygen to Titan's atmosphere actually dates back to the discovery of CO_2 by Voyager (Samuelson et al., 1981). Indeed, carbon dioxide, which also undergoes a condensation sink, was quickly recognized as being formed from reactions between CO and OH, the latter being presumably produced from the photolysis of water. This view was supported by the ground-based discovery of CO (Lutz et al., 1983) and numerous subsequent measurements confirming its large abundance (~50 ppm). Meteoritic ablation was identified as a plausible source of water (Yung et al., 1984; English et al., 1996). Early Titan photochemical models (Samuelson et al., 1983; Yung et al., 1984; Toublanc et al., 1995; Lara et al., 1996) incorporated a source of OH or H_2O, which could be tuned to match the CO_2 abundance, but the ultimate proof of the presence of water had to await its direct detection by ISO/SWS (Coustenis et al., 1998).

The origin of CO in Titan's atmosphere has been the subject of more debate, not only due to controversial results on its vertical distribution (see Gurwell (2004) and references therein), but also to an evolving paradigm on the reaction routes leading to CO. Early photochemical models (Lara et al., 1996, and references therein) assumed that micrometeorite ablation was also the source of CO through the reaction $OH + CH_3 \rightarrow CO + 2H_2$. However, based on laboratory results and first realized by Wong et al. (2002) in the Titan context, this reaction actually proceeds as $OH + CH_3 \rightarrow H_2O + CH_2$ and therefore does not produce CO. Therefore, these authors, as well as the subsequent study by Wilson and Atreya (2004), invoked a surface source (either continuous or primordial) of CO to explain the large CO abundance. Inspired by the Cassini plasma spectrometer (CAPS) discovery of a $\sim 9 \times 10^{23}\ s^{-1}$ (i.e. $\sim 10^6\ cm^{-2}\ s^{-1}$, referred to Titan's surface) influx rate of O^+ (Hartle et al., 2006), Hörst et al. (2008) instead showed that an external source of O or O^+ does lead to the formation of CO, through reaction between ground-state $O(^3P)$ and CH_3. They invoked O/O^+ deposition rates in the range $(0.33–4.2) \times 10^6\ cm^{-2}\ s^{-1}$ (referred to the surface), depending on the assumed eddy diffusion coefficient (K) profile in the lower stratosphere (described by some specific functional form controlled by a K_0 parameter). Comparing with the Hartle et al. (2006) fluxes, they concluded that formation of CO from this process was quantitatively viable, removing the need for a surface or primordial source. The same conclusion was reached later by Krasnopolsky (2009).

Hörst et al. (2008) model is regarded as the most up-to-date and complete model of Titan's oxygen chemistry. They adjusted the OH/H_2O deposition rate, again as a function of K_0, to match the observed CO_2 mixing ratio (15 ppb, vertically uniform over 100–200 km). For a nominal $K_0 = 400\ cm^2\ s^{-1}$, constrained by hydrocarbon profiles (Vuitton et al., 2008), and an OH flux of $2.6 \times 10^6\ cm^{-2}\ s^{-1}$, their model ("model D") yielded a H_2O mole fraction of 3.1×10^{-9} at 400 km. This was deemed to be consistent with the ISO/SWS derived mole fraction of $8^{+6}_{-4} \times \sim 10^{-9}$ at a nominal altitude of 400 km (Coustenis et al., 1998), given the broad vertical extent of the contribution function from the observations. The Hörst et al. (2008) study thus provided an apparently self-consistent picture of the origin of oxygen compounds in Titan's atmosphere, with the three main species (CO, CO_2 and H_2O) being produced from a permanent external supply of oxygen in two distinct forms. However, as it turns out, the Hörst et al. models had not been tested directly against the ISO data. In the previous section, we showed that these models strongly overestimate the unresolved line contrasts observed by Herschel/PACS. In Fig. 8, we show that a similar situation occurs with the two lines observed by ISO/SWS at 43.9 and 39.3 μm, which is not surprising given that these lines essentially have similar optical depths as the PACS data, i.e. probe the same altitudes. Part of the problem is also that, according to our calculations (Fig. 8), the H_2O profile presented in Coustenis et al. (1998) and claimed to fit the ISO/SWS data – i.e. (i) a uniform 4×10^{-10} mole fraction above the saturation level near 12 mbar (ii) the Lara et al. (1996) profile multiplied by a factor of 0.4 – actually strongly overestimate the H_2O emissions seen by ISO/SWS. (We find that a uniform 6×10^{-11} mole fraction or a Lara × 0.083 profile would match the ISO observations). However, as demonstrated in Fig. 7, the problem with the Hörst et al. (2008) and Lara et al. (1996) models is not only in the absolute H_2O amount but also in their shape: these water profiles have respectively too shallow and too steep slopes over 100–300 km (see Fig. 6). In contrast, the best fit profile ("S_a", see Fig. 3) that we inferred from the joint PACS/HIFI analysis does fit well the ISO/SWS lines (Fig. 8), giving further confidence in our model solution. Based on Cassini/CIRS nadir and limb (125 and 225 km tangent altitude) observations of H_2O, Cottini et al. (2012) also find that the models of Lara et al. (1996), and of Hörst et al. (2008) – as well as the model of Wilson and Atreya (2004) – predict inadequate slopes for H_2O (although the Cottini et al. results are quantitatively different from ours. We defer a detailed comparison to future work). All this confirms that photochemical models for water must be revised.

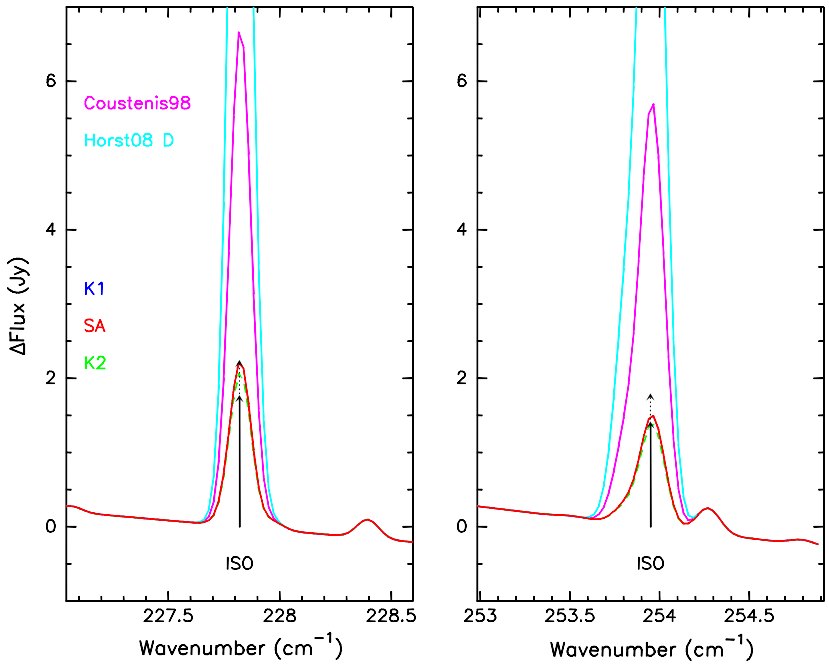

Fig. 8. The ISO observations of H_2O lines at 227.8 cm^{-1} (43.9 μm) and 254.0 cm^{-1} (39.3 μm), compared to various models from previous work (uniform mixing, Lara x 0.4, Hörst A and D), as well as models from this work (S_a, K_1 and K_2). Simulations are convolved by the ISO/SWS spectral resolution of 0.11 and 0.14 cm^{-1}, respectively at 227 and 254 cm^{-1}. The ISO observations are indicated as vertical arrows, including observational error bars (unresolved line contrasts equal to 2 ± 0.25 and 1.6 ± 0.2 Jy, respectively, see Coustenis et al., 1998).

To further explore this aspect, we computed oxygen species profiles using a photochemical model updated from Lara et al. (1996). The model runs from 34 to 1432 km, with a vertical step of 1 km and is suited for low latitudes and moderate solar conditions. Like all other Titan models (Wilson and Atreya, 2004; Hörst et al., 2008; Lavvas et al., 2008; Krasnopolsky, 2009, for the more recent), it is a 1-D model solving the continuity equation. Vertical transport is merely described by eddy and molecular diffusion, with no attempt to account for vertical or horizontal transport due to the general circulation. While Titan's chemistry can be depicted as coupled hydrocarbon, oxygen and nitrogen chemistry, we follow the Lara et al. (1996) approach in which nitrogen chemistry is "decoupled" from the hydrocarbon–oxygen chemistry (as having small effects on the abundance on C-, H- and O-species); in practice, nitrogen-bearing compounds (with the obvious exception of N_2) are simply not included in the model, while the hydrocarbon and oxygen species are solved simultaneously. The same temperature–pressure–profile was adopted as for the radiative transfer calculations presented previously and the two major species (N_2 and CH_4) profiles were held fixed in the model. Hörst et al. (2008) further estimated that the O chemistry does not impact the hydrocarbon profiles, i.e. considered a "background" distribution of the latter, fixed according to the modelling results of Vuitton et al. (2008). Given the new considerations mentioned above, e.g. on the reactions producing CO, oxygen chemistry is entirely updated from Lara et al. (1996) and now prescribed to follow Hörst et al. (2008). In contrast, the hydrocarbon chemistry of Lara et al. is retained, as well as the simplified treatment of aerosol opacity inherited from Yung et al. (1984). As in Lara et al. (1996), lower boundary conditions were prescribed either as fixed mole fractions (this concerns the non-condensible long-lived species CO and H_2, which were prescribed at their observed values, and the condensible compounds for which the saturated abundance at the lower boundary was used), or as resulting from photochemical equilibrium for short-lived species. Diffusion equilibrium was assumed at the upper boundary, except for H and H_2 (Jeans escape). Following Hörst et al. (2008), the photolysis rates were calculated as half the rate for a solar zenith angle of 60°. Numerical convergence was assumed to be reached when successive mole fraction solutions did not differ by more than 1 part in 10^4.

Condensation processes were handled as in Lara et al. (1996), i.e. considering the diffusive growth of ice crystals, as described by Pruppacher and Klett (1980). As elaborated in Lara et al., this formalism allows one to calculate the mass growth rate per crystal, and to infer condensation loss rates. As noted in that paper, the approach requires number density and size profiles for the ice crystals. Although we did not update the aerosol distribution adopted by Lara et al., its influence on the gaseous profiles is negligible, essentially because supersaturation factors are very small (10^{-3}–10^{-6}); in effect, gaseous mole fractions follow their saturation law in the condensation region. Condensation rates calculated in this manner can be compared to the net (i.e. chemical production minus chemical loss), vertically-integrated production rates of the condensing compounds. The agreement is satisfactory (to within 5%) in all cases except for two minor hydrocarbons (CH_3C_2H and to a lesser extent C_4H_2) which have anyway very small condensation rates. In particular, the convergence problems encountered by Lara et al. (1996) for C_2H_6 and H_2O do not occur any more. This primarily stems from the finer altitude grid (1 km here vs 6 km in our previous study), needed to resolve the condensation region.

In a first step, our model calculations were checked against those of Hörst et al. (2008). Fig. 9 shows the vertical profiles of the main oxygen species for conditions of their model D, i.e. adopting their eddy diffusion profile with $K_0 = 400$ cm^2 s^{-1}, an OH flux of 2.6×10^6 cm^{-2} s^{-1} (deposited as a Chapman layer peaking at 750 km), and an O(^{3}P) flux of 1.6×10^6 cm^{-2} s^{-1} (peaking at 1100 km). Instead of solving for the balance of the CO production and loss terms, we specified CO = 5.1×10^{-5} at 34 km, ensuring an adequate CO profile throughout the stratosphere and above. In spite of the different thermal profiles, Fig. 9 compares very well with Fig. 3 of Hörst et al. (2008) for all species. Note, however, that

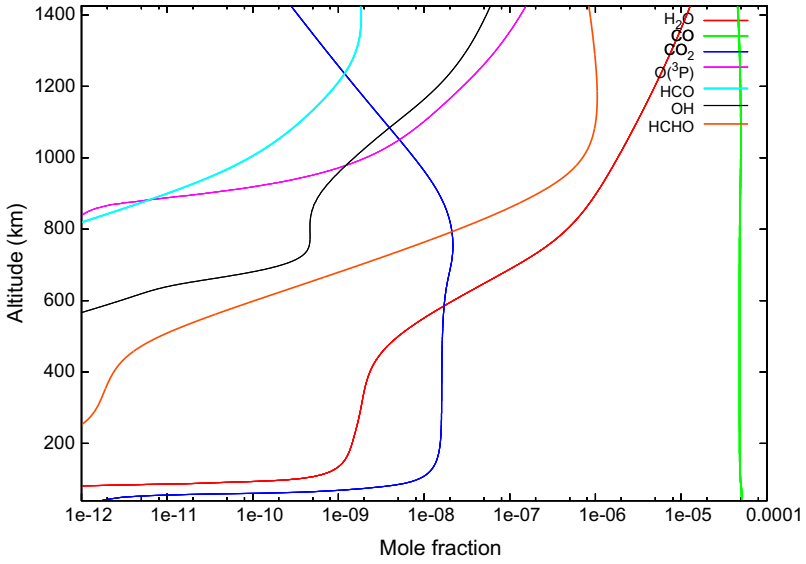

Fig. 9. Calculated oxygen species mole fractions for the conditions of model D of Hörst et al. (2008), i.e. their eddy diffusion profile with $K_0 = 400\ cm^2\ s^{-1}$, an OH flux of $2.6 \times 10^6\ cm^{-2}\ s^{-1}$ deposited as a Chapman layer peaking at 750 km, and an $O(^3P)$ flux of $1.6 \times 10^6\ cm^{-2}\ s^{-1}$ (peaking at 1100 km). This figure is to be compared with Fig. 3 of Hörst et al. (2008).

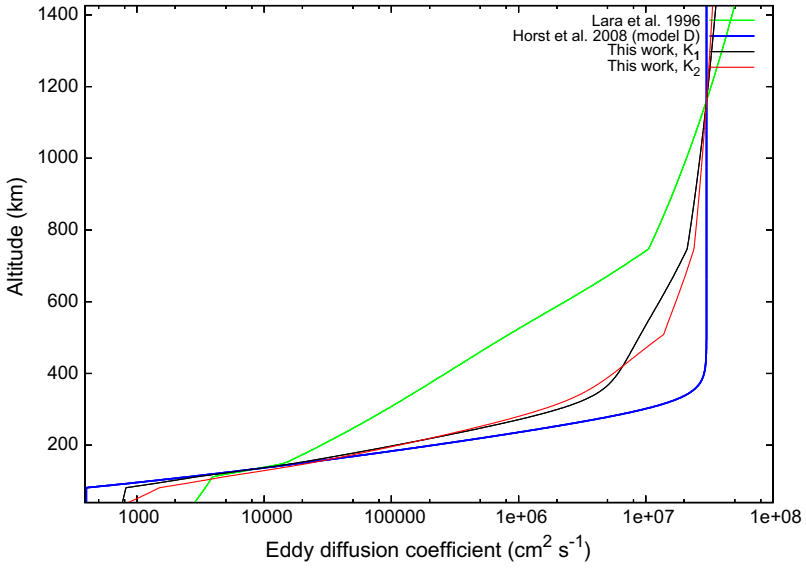

Fig. 10. The two eddy diffusion coefficient profiles (K_1 and K_2) considered in this work and in previous papers (Lara et al., 1996; Hörst et al., 2008, model D).

in our calculations and for an $O(^3P)$ flux of $1.6 \times 10^6\ cm^{-2}\ s^{-1}$, the CO production exceeds its loss by 37%. In other words, we find that the observed CO abundance is not in equilibrium with an $O(^3P)$ flux of $1.6 \times 10^6\ cm^{-2}\ s^{-1}$. Balance would be achieved for an $O(^3P)$ flux of $0.85 \times 10^6\ cm^{-2}\ s^{-1}$, still (and even more) consistent with the Cassini/CAPS measurements of Hartle et al. (2006). This difference with the results of Hörst et al. is unconsequential for our issue, as the OH, H_2O and CO_2 profiles are entirely unaffected by the $O(^3P)$ flux as long as the CO is held fixed to its observed value.

The eddy K profile of Hörst et al. (2008) (see Fig. 10) derives from Vuitton et al. (2008), who used as a constraint the C_2H_2 and C_2H_6 profiles retrieved by Vinatier et al. (2007) from Cassini/CIRS measurements at 15S. Additional profiles at 5N and 20S were presented by Vinatier et al. (2010), using in particular a new line list for C_2H_6. They are shown along with the 15S profiles in Fig. 11. In this figure, the C_2H_6 profile at 15S has been updated to account for the new line list, resulting in a ~40–50% decrease from the original Vinatier et al. (2007) profile. Our model calculations using the Hörst et al. (2008) eddy K profile lead us to overestimate the C_2H_2 and C_2H_6 profiles, by mean factors of ~1.65 and 1.7 respectively. This can be fixed by decreasing uniformly the production rates of the two species by factors of 1.11 and 1.47. However, the resulting vertical profile of C_2H_6 (black line in Fig. 11) is not satisfactory, showing not enough increase with altitude, especially over 150–300 km. On the other hand, the C_2H_2 profile is very well fit up to 250 km (dark blue[1] line in Fig. 11). These behaviors can also be seen in the results from Vuitton et al. (2008) (their Fig. 11), showing an excellent fit of C_2H_2, yet a clear overestimate of C_2H_6 below 250 km. The mismatch on ethane leads us to conclude that their eddy K is too large over 150–400 km. This conclusion is qualitatively consistent with the fact that

[1] For interpretation of color in Figs. 9–13, the reader is referred to the web version of this article.

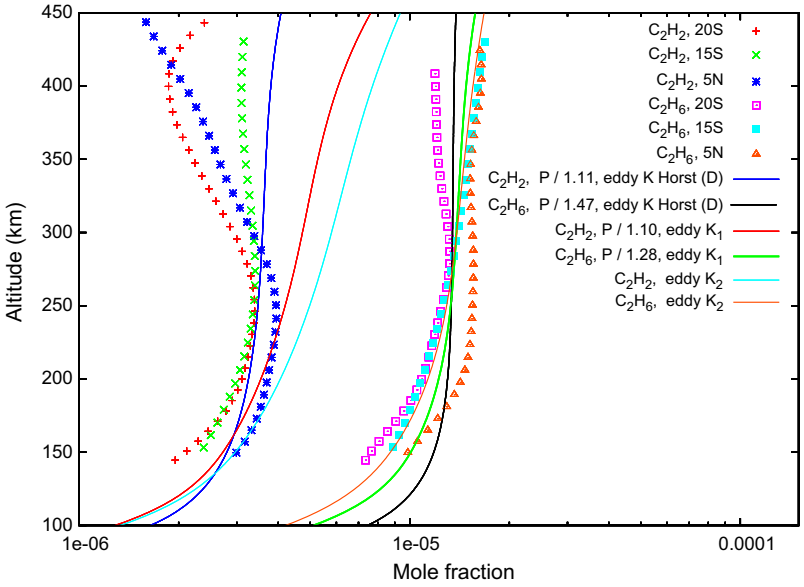

Fig. 11. Low-latitude ethane and acetylene vertical profiles, inferred from Cassini/CIRS measurements, and compared with photochemical model calculations. Profiles at 5N and 20S are from Vinatier et al. (2010), while profile at 15S is updated from Vinatier et al. (2007) (see text). Eddy diffusion profiles K_1, K_2 from this work and D from Hörst et al. (2008) are considered. In the case of K_1 and D profiles, reduction factors for the production rates are applied as indicated.

the Hörst et al. (2008) models do not show a sufficient decrease of H_2O with increasing pressure.

We therefore explored eddy K profiles intermediate between those of Hörst et al., 2008 (model D, K_h) and Lara et al. (1996) (K_l), using numerical combinations of those. We found that a profile defined by $K_1 = K_h^{2/3} K_l^{1/3}$ provides a satisfactory fit to the C_2H_6 slope (Fig. 11), and as discussed hereafter a good fit to the HIFI and PACS observations of H_2O. In Fig. 11, the production rates of C_2H_2 and C_2H_6 have been still decreased by factors of 1.10 and 1.28, respectively, to improve the match to their absolute abundances. The associated eddy profile is shown in Fig. 10 along with the original K_h and K_l profiles. The "price to pay" with this new K_1 profile is a degradation of the fit of C_2H_2 above 250 km. Note however that the Vinatier et al. (2010) C_2H_2 profiles at 5N and 20S seem to show a decrease of the mole fractions with altitude above 250 km, which might result from dynamical effects not amenable to a simple vertical eddy diffusion. Therefore, it seems reasonable to use the C_2H_6 profile as the best constraint for the eddy diffusion profile. This approach was previously used by Lara et al. (1999) and Vinatier et al. (2007) to demonstrate the loss of HCN to the haze. Although the latter authors assumed no chemical production or loss in the altitude region of interest, which is not correct (Krasnopolsky, 2009). Continuing with this approach, but now without any tuning of the hydrocarbon production rates, we determined the eddy K profile ("K_2", red curve in Fig. 10) optimizing the fit to C_2H_6. This case however further degrades the fit to C_2H_2, so both the K_1 and K_2 profiles were considered in the following.

Oxygen species profiles calculated with the K_1 profile are shown in Fig. 12. We leave the $O(^3P)$ flux unchanged at 1.6×10^6 cm^{-2} s^{-1}, but the OH influx, still deposited in the form of a Chapman layer with peak at 750 km, has been multiplied by a factor 0.13 (input flux 3.4×10^5 cm^{-2} s^{-1}). Besides the lower H_2O abundance at all altitudes, the most obvious change compared to Fig. 9 is the more steady decline of H_2O below 400 km. This results mostly from the change of eddy K, but also from the decrease by a factor ~2 of C_2H_2 below 250 km, which leads to the increase of the photolysis of H_2O at long wavelengths. Similar results are shown in Fig. 13 for eddy K_2. In this model, in addition to the change in the assumed eddy K profile, the OH influx is specified as a flux boundary condition at the top of the atmosphere. This mimicks the case, for which we argue below, that a plausible source of oxygen for Titan is the Enceladus water torus, a situation in which water would enter Titan's atmosphere in gaseous (OH + H_2O) form at the top of the atmosphere. In this case, the required OH flux is 2.7×10^5 cm^{-2} s^{-1} (still referred to the surface), a 20% decrease from the previous case. Mole fractions in Figs. 12 and 13 are very similar, except of course for OH due to its different source location, and for small changes in the upper part of the H_2O profile. The OH vs H_2O form of the water input is also unimportant (since a balance establishes between OH and H_2O, due to the photolysis of water and reactions between OH and CH_3 or OH and CH_4 recycling water).

As demonstrated in Figs. 5 and 8, the water profiles of Figs. 12 and 13 (also shown in Fig. 6) now fit all the HIFI and PACS observations simultaneously, and also agree with the ISO observations of Coustenis et al. (1998). Note in Fig. 6 that in both of these models, the H_2O mole fraction at 1000–1100 km is consistent with the INMS upper limit averaged over 15 flybys ($< 3 \times 10^{-6}$, Cui et al. (2009)), while previous distributions by Coustenis et al. (1998) and Hörst et al. (2008) tend to overestimate the H_2O thermospheric mole fraction. We conclude that the OH flux required to match the Herschel H_2O observations is $(2.7–3.4) \times 10^5$ cm^{-2} s^{-1}. Note also that with these $O(^3P)$ and OH influxes and the adopted eddy K profiles, we find that the CO production exceeds its loss by a large factor (7.5) – due to the much lower OH abundance compared to the Hörst et al. (2008) models – and that chemical balance for CO = 5.1×10^{-5} would be achieved for an $O(^3P)$ flux of only ~1.3×10^5 cm^{-2} s^{-1}. Once again, this has no impact on the OH flux requirement for H_2O. Moreover, this is of little significance as the CO abundance results from its production/loss balance over hundreds of millions of years, while the H_2O abundance builds from OH over a timescale of ~10 years only (see below). In other words, this does not mean that the CO ~50 ppm abundance is inconsistent with a current $O(^3P)$ flux of ~10^6 cm^{-2} s^{-1}, as estimated from Cassini/CAPS.

As is clear from Figs. 12 and 13, a ~3×10^5 cm^{-2} s^{-1} OH/H_2O input leads to a CO_2 mole fraction of $(1–2) \times 10^{-9}$, an order of magnitude short below the observed value. Restoring a 1.5×10^{-8} mole fraction for CO_2 over 100–200 km would require an OH influx of

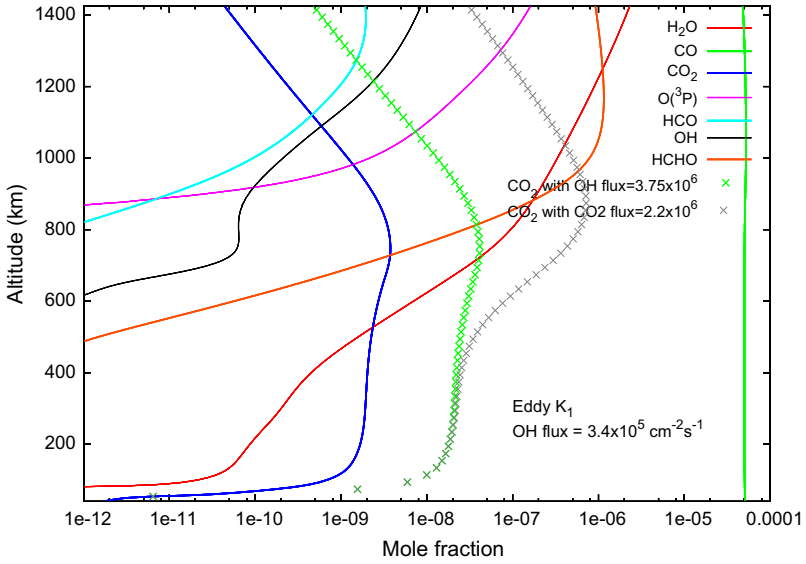

Fig. 12. Solid lines: calculated oxygen species mole fractions for eddy diffusion K_1 model and an OH flux of 3.4×10^5 cm^{-2} s^{-1}, referred to the surface, deposited in the form of a Chapman layer peaking at 750 km. Green points: the CO_2 profile calculated with an OH flux of 3.75×10^6 cm^{-2} s^{-1}. Gray points: the CO_2 profile calculated by assuming deposition of combined OH (3.4×10^5 cm^{-2} s^{-1}) and CO_2 (2.2×10^6 cm^{-2} s^{-1}) fluxes.

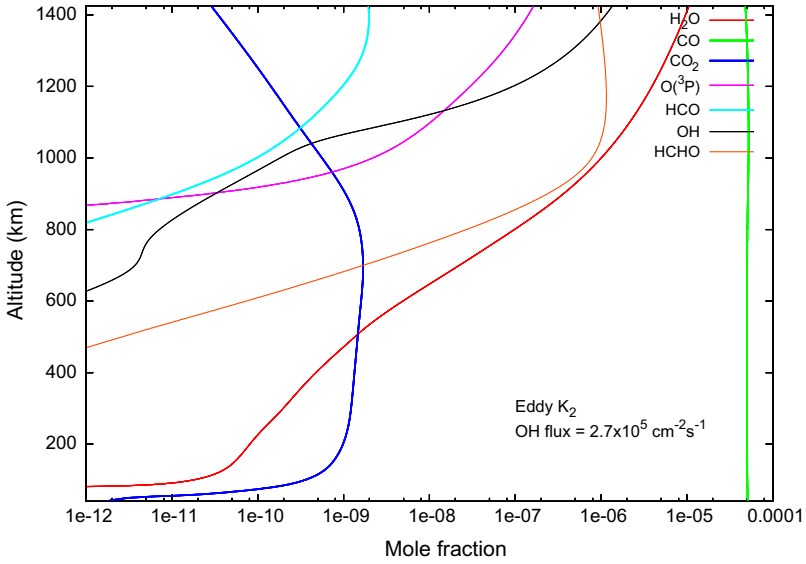

Fig. 13. Calculated oxygen species mole fractions for eddy diffusion K_2 model and an OH flux of 2.7×10^5 cm^{-2} s^{-1}, referred to the surface, deposited at the top of the atmosphere. Although the OH profile is very different from the case of Fig. 12, the H_2O profile is very similar up to ~800 km, and both models fit the Herschel HIFI/PACS observations equally well (see Fig. 5).

~3.7×10^6 cm^{-2} s^{-1} (for the case of model K_1, green points in Fig. 12), roughly ~10 times larger than required for H_2O. Ways out of this dilemma are not obvious. Direct injection of CO_2 (e.g. from micrometeoritic ablation) has been envisaged to explain the presence of CO_2 in the Giant Planets (Feuchtgruber et al., 1997; Moses et al., 2000). There this scenario requires a plausible CO_2/H_2O ratio in the incoming grains, roughly consistent with cometary composition. This explanation, however, is probably not viable at Titan, where the atmospheric CO_2/H_2O ratio is much larger than in the Giant Planets. Specifically, assuming also for CO_2 that deposition occurs in a Chapman layer with peak at 750 km, an additional huge CO_2 flux of 2.2×10^6 cm^{-2} s^{-1} (i.e. ~7 times larger than the OH flux) would be required (gray points in Fig. 12). As CO_2 condenses at tropopause temperatures, and although CO_2 ice evaporating from Titan's surface following the Huygens landing has been reported (Niemann et al., 2010), a surface source of CO_2 does not seem to offer a solution.

Another plausible explanation that might warrant consideration would be that H_2O involves additional chemical losses than those considered here. Non-gaseous losses for HCN (i.e. to the haze) have been advocated first by McKay (1996) on the basis of laboratory-based estimates of the C/N ratio in the haze, then also in the framework on a photochemical model by Lara et al. (1999) and more recently by Vinatier et al. (2007). In the latter two papers, it was found that a non-gaseous HCN loss rate of a few 10^8 cm^{-2} s^{-1} would reconcile the HCN and C_2H_6 profiles, i.e. allow both species to be fit by the same eddy K profile. Whether a similar process could occur for H_2O is anything but speculative. Coming back to the favored model of Hörst et al. (2008) (i.e. their eddy K and a OH deposition of 2.6×10^6 cm^{-2} s^{-1}), we found that an

approximate fit of the H_2O distribution can be achieved by assuming an additional H_2O loss in the form $L = 3 \times 10^{-12}[H_2O]^{1.75}$ cm^{-3} s^{-1}, restricted to altitudes above 220 km, i.e. a total loss of 1.9×10^6 cm^{-2} s^{-1}. However, not surprisingly given that the formation of CO_2 occurs predominantly from OH, the associated CO_2 profile remains inadequate, with values of only $(2–3) \times 10^{-9}$ at 150–200 km. Thus, this avenue does not seem promising.

5. Discussion and the origin of water in Titan's atmosphere

Based on the vertical distribution of water and photochemical modelling, we determine that the OH input flux required to explain the H_2O abundance and profile is $\sim 3 \times 10^5$ cm^{-2} s^{-1}, typically 10 times less than needed for the observed CO_2 abundance. A plausible explanation for the very different flux may be found by accounting for their vastly different atmospheric lifetimes. Wilson and Atreya (2004) find a factor-of-170 longer lifetime above 300 km for CO_2 compared to H_2O. In our model K_1, the H_2O column density is 1.25×10^{14} cm^{-2} (referred to surface), and its production and chemical loss are approximately equal (i.e. the condensation loss is essentially negligible) at 4.3×10^5 cm^{-2} s^{-1}. Dividing the H_2O column density by the chemical loss indicates a global atmospheric lifetime of ~9 years (consistent with the estimate given in Coustenis et al. (1998)). Such a H_2O lifetime is consistent with the fact that we do not detect any variations in the H_2O abundance between the leading and trailing sides, nor in observations taken over a ~1-year interval (Fig. 1a, d, and e), and also on a timescale of 13 years between the Herschel and ISO observations. However, the CO_2 lifetime is even much longer: for models matching the 15 ppb CO_2 mole fraction (see Figs. 12 and 13), the CO_2 column density is 3.6×10^{16} cm^{-2}, and loss rate is 2.5×10^6 cm^{-2} s^{-1} (~80% of which being due to vertical transport followed by condensation). The ratio of the two numbers indicates a lifetime of 450 years. A similar number (360 years) is obtained from the vertical transport lifetime down to the condensation level near 100 km, defined by $\tau = 2H^2/K$, where H (~32 km) and K (~1800 cm^2 s^{-1}) are the atmospheric scale height and eddy diffusion coefficient near 100 km, respectively. This consideration means that the H_2O atmospheric abundance will react to mid-term (~10 year) variability of the external source, while the CO_2 will reflect its mean value over centuries. If true, this interpretation would imply that the current external supply of H_2O/OH to Titan is typically smaller by an order-of-magnitude than its characteristic value over the last centuries.

Since the H_2O lifetime is moderately shorter than a Titan year, this leaves also open the possibility than H_2O could, unlike CO_2 (e.g. Coustenis et al., 2010) shows a non-uniform latitudinal distribution, variable on seasonal timescales. Cassini/CIRS spectra of H_2O reported by Cottini et al. (2012) do no show evidence for such horizontal variations, however. This implies a meridional mixing timescale shorter than the chemical timescale.

The OH/H_2O input flux we determine is lower than all previous estimates (see Hörst et al., 2008; Strobel et al., 2010, and references therein), which spanned the range 6×10^5–9×10^6 cm^{-2} s^{-1}, with most values higher than 1.5×10^6 cm^{-2} s^{-1}. As noted by Coustenis et al. (1998) and Moses et al. (2000), these values were surprisingly high when compared to the required flux into Saturn, $(0.5–2) \times 10^6$ cm^{-2} s^{-1} according to Moses et al., consistent with 1×10^6 cm^{-2} s^{-1} from Ollivier et al. (2000). As calculated in Moses et al. (2000), if the OH/H_2O flux into the outer planets is dominated by interplanetary dust particles (IDP), Saturn should capture significantly more material than Titan due to its gravitational focusing effect, by factors 6–16 depending on the orbit of the IDPs (i.e. comet-like or Kuiper-Belt). Interstellar grains should also favor Saturn over Titan, albeit by a smaller factor (~3). Our result of a much lower OH/H_2O input flux into Titan alleviates this problem considerably: using nominal estimates of 3×10^5 cm^{-2} s^{-1} for Titan and 1.5×10^6 cm^{-2} s^{-1} for Saturn now gives a Saturn/Titan flux ratio of 5, plausibly accounted for by the differential gravitational effect of Saturn. In absolute terms, based on their estimate of the total O flux into Saturn, Moses et al. (2000) determine that, to account for Saturn's oxygen compounds, the unfocused dust flux at Saturn must be in the range $(0.2–4) \times 10^{-17}$ g cm^{-2} s^{-1} for IDP (depending on grain orbit) and $\sim 1 \times 10^{-16}$ g cm^{-2} s^{-1} for instellar grains. Given that the unfocused flux at Earth's orbit is 1.2×10^{-16} g cm^{-2} s^{-1} (Love and Brownlee, 1993) and that the interplanetary fluxes decrease roughly by a factor of 10 from the Earth to Jupiter and remain approximately constant beyond (Landgraf et al., 2002), the above range is consistent with interplanetary dust (but not interstellar dust) being at the origin of Saturn's oxygen compounds and Titan's water.

In a variant of the IDP source hypothesis, Krivov and Banaszkiewicz (2001) have shown that icy material ejected from Hyperion (either by IDP impact, or indirectly, by Phoebe dust, itself produced from IDP collisions) provides a source comparable in magnitude to the direct influx of IDPs to Titan. In all these cases, material would enter Titan's atmosphere in the form of icy dust grains undergoing ablation at an altitude depending on their entry velocity (and direction). The typical ablation altitude is near 750 km for IDPs (English et al., 1996) and should be slightly deeper for Hyperion grains whose encounter velocity is significantly smaller (2–4 km/s, Krivov and Banaszkiewicz, 2001)

Based on the detection of the Enceladus H_2O torus with Herschel/HIFI, Hartogh et al. (2011) have proposed instead that Enceladus' plume activity may be at the origin of Saturn's water. Indeed, combining the column-integrated H_2O amounts measured by Herschel in the torus with a transport model tracking the fate of H_2O molecules emitted by Enceladus' vents (Cassidy and Johnson, 2010), Hartogh et al. showed that their observations indicated an Enceladus source rate of 0.85×10^{28} s^{-1} – well in line with estimates from Cassini at plume level (see below) – and a OH/H_2O influx rate into Saturn of $\sim 6 \times 10^5$ cm^{-2} s^{-1}, encompassing the required $(0.5–2) \times 10^6$ cm^{-2} s^{-1} flux range. The estimated flux rate into Titan is $\sim 4 \times 10^5$ OH/H_2O cm^{-2} s^{-1} and $\sim 1 \times 10^6$ O cm^{-2} s^{-1}, where the larger value for O is due to the more extended atomic O torus. Comparing with the requirements of the Hörst et al. (2008) model, Hartogh et al. (2011) concluded that Enceladus was providing enough atomic O to account for Titan CO, but failed to explain Titan water. With our new estimate of the OH/H_2O flux into Titan, this option now becomes viable as well. As seen from Titan, the essential difference with the IDP (and its Hyperion variant) scenario is that for an Enceladus source, water will enter Titan in gaseous form at the top of the atmosphere.

Both the direct IDP and the Enceladus sources are expected to produce a much larger deposition rate on Titan's leading vs trailing side, as a result of the orbits of dust (IDP) or gas (Enceladus) material impacting Titan. Calculated lead/trail contrasts in the H_2O/OH deposition rate are a factor of 20 for IDPs (English et al., 1996) and on the order of 30 for the Enceladus source (Cassidy and Johnson, 2010); in this latter case, this is due to the fact that most atoms/molecules emitted by Enceladus are slower than Titan when they cross its orbit, a consequence of their being on eccentric orbits with periapse near Enceladus' orbit. In contrast, Krivov and Banaszkiewicz (2001) find that the asymmetry in deposition profiles is much smaller in the case of the Hyperion dust case, with a lead/trail contrast of 1.3–2 only. In any case, as mentioned above, the long (column-integrated) lifetime of water (~9 years) compared to diurnal or dynamical timescales (16 terrestrial days for Titan's rotation, and about 1 terrestrial day for longitudinal hemispheric transport at a typical zonal velocity of ~100 m/s) provides a natural explanation for the absence of lead/trail contrast in

Titan's water (Fig. 1d and e). Hence this homogeneity cannot be used to discriminate between a source sharply peaked towards Titan's leading side, or a source more evenly distributed over Titan longitudes. From the observational point of view, separating the IDP, Enceladus, and Hyperion sources would probably require determining the H_2O vertical profile up to ~900 km (see Figs. 12 and 13), which could be achieved through limb observations from a Titan orbiter equipped with a submillimeter instrument (Lellouch et al., 2010).

We are thus left with two types of sources, equally viable in terms of flux, for Titan external water. In both cases, our above interpretation of the different fluxes required to explain Titan's H_2O and CO_2 implies a large, factor-of-10 variation of the source, on timescales of tens of years to centuries. Obviously, neither the IDP flux nor Enceladus' activity have been documented on such periods. In particular, the (indirect) detection of the Enceladus source dates back only to 1992, with the discovery of the OH in Saturn's magnetosphere from the Hubble Space Telescope (HST) (Shemansky et al., 1993). Observations from Cassini over the last few years have led to somewhat conflicting results as to the time variability of plume activity. Analysis of INMS data suggested significant variations between the E2, E3, E5 and E7 encounters, by at least a factor 4 (6×10^{27}–2.5×10^{28} s^{-1} according to Smith et al. (2010)), but only by a factor of ~2 (1.5×10^{28}–3.5×10^{28} s^{-1} according to Dong et al. (2011)). An even larger, factor-of-8, variability was reported from the analysis of magnetic field data over E0–E2 (Saur et al., 2008). In contrast, the interpretation of Cassini's UltraViolet Imaging Spectrograph (UVIS) occultations (Hansen et al., 2006; Tian et al., 2007; Burger et al., 2007) points to a very limited source variability (~15%, on a mean value of $\sim 0.7 \times 10^{28}$ s^{-1} (Hansen et al., 2011). Regarding the OH observations, modelling by Jurac and Richardson (2005); Cassidy and Johnson (2010); and Melin et al. (2009) indicates that a "standard" source rate of 1×10^{28} s^{-1} is able to match the OH column densities measured over 1992–1996, while also fitting the abundance of atomic O, discovered and measured by Cassini/UVIS (Esposito et al., 2004; Melin et al., 2009). Based on all this, and the remarkable stability of the H_2O absorption seen by Herschel over 2009–2010 (Hartogh et al., 2011), there is no clear evidence for any variability of Enceladus plume activity in the last two decades. This does not seem to preclude the possibility that Enceladus' activity was more intense over the last few centuries than currently. In fact, while active plumes are associated with thermal anomalies along "tiger stripes" fractures near Enceladus South poles (e.g. Spitale et al., 2007), it is noteworthy that (i) plumes are not emitted along entire fractures (ii) thermal anomalies extend beyond fractures (Spencer et al., 2011). This leaves the possibily of more extended and intense activity in a recent past. On the other hand, it would a priori seems less likely that the IDP fluxes at Saturn and Titan show large variations over timescales of centuries. Indeed, although IDP production rate from comets may be variable, dust fluxes at 10 AU seem to be dominated by Kuiper-Belt dust (i.e. produced by mutual collisions between Kuiper-Belt objects and/or from impacts of interstellar grains on their surfaces) with cometary activity (from short-period Jupiter-family and Halley-type comets) providing only secondary, albeit not negligible, contribution (Landgraf et al., 2002).

We finally note that whatever the source, if variable, its variability will affect Saturn's oxygen compounds as well. In Saturn's atmosphere also, CO_2 has a much longer lifetime than that of H_2O. This means that fitting Saturn's CO_2 and H_2O current abundances may not necessarily require the same flux of oxygen species. In this respect, a remarkable result from Moses et al. (2000) is that it is not possible to fit all three oxygen compounds (CO, CO_2, H_2O) with oxygen in a single molecular form. We leave aside CO, which apparently results from a sporadic cometary event a few hundreds years ago (Cavalié et al., 2010). Nonetheless, Moses et al. find that when a pure H_2O source is considered and tuned to match Saturn's H_2O, the photochemically produced CO_2 is a factor-of-7 too small to explain the ISO observations, a factor strikingly similar to the Titan situation. While they invoke simultaneous precipitation of C–O bearing material consistent with cometary composition, the explanation we offer for Titan – calling for a currently low H_2O input compared to its typical value over the last centuries – would seem to work also for Saturn. Our tentative conclusion is thus that a variable Enceladus activity might be the cause of the unexpectedly large CO_2/H_2O ratio on both Saturn and Titan.

6. Summary

In the framework of the Key Programme "Water and related chemistry in the Solar System" of Herschel, we have performed dedicated observations of several rotational lines of water in Titan's atmosphere, using both PACS (at 66.4, 75.3 and 108.0 μm) and HIFI (at 557 and 1097 GHz), covering several periods in June 2010, December 2010 and June 2011. The main findings on this study can be summarized as follows:

(i) Lines for which we have multiple observations (primarily the 66.4 μm line) do not show any significant variability (within 10%) over a ~1 year interval, nor between Titan's leading and trailing sides.

(ii) The spectrally-resolved HIFI observations indicate that the H_2O lines at 557 and 1097 GHz are narrow (FWHM ~ 2–4 MHz), implying a strong positive gradient of the H_2O mole fraction above the 12 mbar condensation level (i.e. in the 93–450 km range).

(iii) This behavior is confirmed by the relative contrast of the various lines observed by HIFI and PACS. Fitting the ensemble of data with a semi-empirical profile is achieved with a best fit mole fraction $q = (2.3 \pm 0.6) \times 10^{-11}$ at 12.1 mbar and a slope $-d(\ln q)/d(\ln p) = 0.49 \pm 0.07$, corresponding to a H_2O column density of $(1.2+/-0.2) \times 10^{14}$ cm^{-2}.

(iv) H_2O profiles proposed from previous photochemical models – tuned to fit either the CO_2 abundance or the original H_2O lines detected by ISO (Coustenis et al., 1998) – are too water-rich to match the Herschel observations, nor do they have the appropriate shape. In particular, the water profiles of Lara et al. (1996) and Hörst et al. (2008) are too steep and too shallow, respectively, in the lower stratosphere.

(v) Based on an update of the Lara et al. (1996) photochemical model, in which the eddy diffusion coefficient is constrained by the C_2H_2 and C_2H_6 vertical distribution, we fit the Herschel dataset with an OH/H_2O input flux of $(2.7–3.4) \times 10^5$ - mol cm^{-2} s^{-1}, referred to the surface.

(vi) Both the semi-empirical and photochemically-derived profiles fitting the Herschel data also match the H_2O ISO observations.

(vii) The required OH/H_2O flux is essentially one order of magnitude lower than invoked by previous modellers, and also a factor of ~10 less than required to match the observed CO_2 mole fraction.

(viii) We propose that this apparent contradiction is due to the fact that, in relation to its atmospheric lifetime (~9 years), H_2O reacts to variations of the input flux on timescales much shorter than CO_2 (~450 years), and we suggest that this flux is currently ~10 times smaller than averaged over the last centuries

(ix) A $\sim 3 \times 10^5$ mol cm^{-2} s^{-1} OH/H_2O flux is consistent both with estimates of (i) the IDP flux at Saturn's distance and (ii) the input flux into Titan due to Enceladus plume activity

(for a standard source rate of $\sim 1 \times 10^{28}$ s^{-1}). The two types of sources may differ in the associated deposition profile, eventually leading to different H_2O abundances in the upper atmosphere (>700 km), but those are so far poorly constrained by observations. Nonetheless, we tentatively favor the Enceladus source as potentially more prone to time variability.

Acknowledgments

We acknowledge very useful discussions with B. Bézard. This work has been supported by the French Programme Nationale de Planétologie (PNP). L.M. Lara's work has been supported by the Ministry of Innovation and Science through the project AyA 2009-08011. The MPS contribution has been supported by the grant of the German Research Foundation DFG HA 3261/7-1.

HIFI has been designed and built by a consortium of institutes and university departments from across Europe, Canada and the United States under the leadership of SRON Netherlands Institute for Space Research, Groningen, The Netherlands and with major contributions from Germany, France and the US. Consortium members are: Canada: CSA, U.Waterloo; France: CESR, LAB, LERMA, IRAM; Germany: KOSMA, MPIfR, MPS; Ireland, NUI Maynooth; Italy: ASI, IFSI-INAF, Osservatorio Astrofisico di Arcetri-INAF; Netherlands: SRON, TUD; Poland: CAMK, CBK; Spain: Observatorio Astronmico Nacional (IGN), Centro de Astrobiologa (CSIC-INTA). Sweden: Chalmers University of Technology – MC2, RSS and GARD; Onsala Space Observatory; Swedish National Space Board, Stockholm University – Stockholm Observatory; Switzerland: ETH Zurich, FHNW; USA: Caltech, JPL, NHSC.

PACS has been developed by a consortium of institutes led by MPE (Germany) and including UVIE (Austria); KUL, CSL, IMEC (Belgium); CEA, OAMP (France); MPIA (Germany); IFSI, OAP/AOT, OAA/CAISMI, LENS, SISSA (Italy); IAC (Spain). This development has been supported by the funding agencies BMVIT (Austria), ESA-PRODEX (Belgium), CEA/CNES (France), DLR (Germany), ASI (Italy), and CICYT/MCYT (Spain).

References

Anderson, C.M., Samuelson, R.E., 2011. Titan's aerosol and stratospheric ice opacities between 18 and 500 μm: Vertical and spectral characteristics from Cassini CIRS. Icarus 212, 762–778.

Bézard, B., 2009. Composition and chemistry of Titan's stratosphere. R. Soc. Lond. Philos. Trans. Ser. A 367, 683–695.

Bézard, B., Lellouch, E., Strobel, D., Maillard, J.-P., Drossart, P., 2002. Carbon monoxide on Jupiter: Evidence for both internal and external sources. Icarus 159, 95–111.

Borysow, A., Frommhold, L., 1986. Collision-induced rototranslational absorption spectra of N_2–N_2 pairs for temperatures from 50 to 300 K. Astrophys. J. 311, 1043–1057.

Borysow, A., Frommhold, L., 1987. Collision-induced rototranslational absorption spectra of CH_4–CH_4 pairs at temperatures from 50 to 300 K. Astrophys. J. 318, 940–943.

Borysow, A., Tang, C., 1993. Far infrared CIA spectra of N_2–CH_4 pairs for modeling of Titan's atmosphere. Icarus 105, 175–183.

Burger, M.H., Sittler, E.C., Johnson, R.E., Smith, H.T., Tucker, O.J., Shematovich, V.I., 2007. Understanding the escape of water from Enceladus. J. Geophys. Res. (Space Phys.) 112, A06219.

Cassidy, T.A., Johnson, R.E., 2010. Collisional spreading of Enceladus' neutral cloud. Icarus 209, 696–703.

Cavalié, T. et al., 2010. A cometary origin for CO in the stratosphere of Saturn? Astron. Astrophys. 510, A88.

Cazzoli, G., Puzzarini, C., Buffa, G., Tarrini, O., 2009. Pressure-broadening of water lines in the THz frequency region: Improvements and confirmations for spectroscopic databases – Part II. J. Quant. Spectrosc. Radiat. Trans. 110, 609–618.

Cottini, V., Nixon, C.A., Jennings, D.E., Anderson, C.M., Gorius, N., Bjoraker, G.L., Coustenis, A., Teanby, N.A., Achterberg, R.K., Bézard, B., de Kok, R., Lellouch, E., Irwin, P.G.J., Flasar, F.M., Bampasidis, G., 2012. Water vapor in Titan's stratosphere from Cassini CIRS far-infrared spectra. Icarus 220, 855–862.

Courtin, R. et al., 2011. First results of Herschel-SPIRE observations of Titan. Astron. Astrophys. 536, L2.

Coustenis, A. et al., 1998. Evidence for water vapor in Titan's atmosphere from ISO/SWS data. Astron. Astrophys. 336, L85–L89.

Coustenis, A., Jennings, D.E., Nixon, C.A., Achterberg, R.K., Lavvas, P., Vinatier, S., Teanby, N.A., Bjoraker, G.L., Carlson, R.C., Piani, L., Bampasidis, G., Flasar, F.M., Romani, P.N., 2010. Titan trace gaseous composition from CIRS at the end of the Cassini–Huygens prime mission. Icarus 207, 461–476.

Cui, J., Yelle, R.V., Vuitton, V., Waite, J.H., Kasprzak, W.T., Gell, D.A., Niemann, H.B., Müller-Wodarg, I.C.F., Borggren, N., Fletcher, G.G., Patrick, E.L., Raaen, E., Magee, B.A., 2009. Analysis of Titan's neutral upper atmosphere from Cassini Ion Neutral Mass Spectrometer measurements. Icarus 200, 581–615.

de Graauw, T. et al., 2010. The Herschel–Heterodyne Instrument for the Far-Infrared (HIFI). Astron. Astrophys. 518, L6.

de Kok, R., Irwin, P.G.J., Teanby, N.A., Nixon, C.A., Jennings, D.E., Fletcher, L., Howett, C., Calcutt, S.B., Bowles, N.E., Flasar, F.M., Taylor, F.W., 2007. Characteristics of Titan's stratospheric aerosols and condensate clouds from Cassini CIRS far-infrared spectra. Icarus 191, 223–235.

Dong, Y., Hill, T.W., Teolis, B.D., Magee, B.A., Waite, J.H., 2011. The water vapor plumes of Enceladus. J. Geophys. Res. (Space Phys.) 116, A10204.

English, M.A., Lara, L.M., Lorenz, R.D., Ratcliff, P.R., Rodrigo, R., 1996. Ablation and chemistry of meteoric materials in the atmosphere of Titan. Adv. Space Res. 17, 157–160.

Esposito, L.W. et al., 2004. The Cassini ultraviolet imaging spectrograph investigation. Space Sci. Rev. 115, 299–361.

Feuchtgruber, H., Lellouch, E., de Graauw, T., Bézard, B., Encrenaz, T., Griffin, M., 1997. External supply of oxygen to the atmospheres of the Giant Planets. Nature 389, 159–162.

Fulchignoni, M. et al., 2005. In situ measurements of the physical characteristics of Titan's environment. Nature 438, 785–791.

Golubiatnikov, G.Y., Koshelev, M.A., Krupnov, A.F., 2008. Pressure shift and broadening of 1_{10} 1_{01} water vapor lines by atmosphere gases. J. Quant. Spectrosc. Radiat. Trans. 109, 1828–1833.

Griffin, M.J. et al., 2010. The Herschel-SPIRE instrument and its in-flight performance. Astron. Astrophys. 518, L3.

Gurwell, M.A., 2004. Submillimeter observations of Titan: Global measures of stratospheric temperature, CO, HCN, HC_3N, and the isotopic ratios $^{12}C/^{13}C$ and $^{14}N/^{15}N$. Astrophys. J. 616, L7–L10.

Hansen, C.J. et al., 2006. Enceladus' water vapor plume. Science 311, 1422–1425.

Hansen, C.J. et al., 2011. The composition and structure of the Enceladus plume. Geophys. Res. Lett. 38, L11202.

Hartle, R.E. et al., 2006. Initial interpretation of Titan plasma interaction as observed by the Cassini plasma spectrometer: Comparisons with Voyager 1. Planet. Space Sci. 54, 1211–1224.

Hartogh, P. et al., 2009. Water and related chemistry in the Solar System. A guaranteed time key programme for Herschel. Planet. Space Sci. 57, 1596–1606.

Hartogh, P. et al., 2011. Direct detection of the Enceladus water torus with Herschel. Astron. Astrophys. 532, L2.

Hesman, B.E., Davis, G.R., Matthews, H.E., Orton, G.S., 2007. The abundance profile of CO in Neptune's atmosphere. Icarus 186, 342–353.

Hörst, S.M., Vuitton, V., Yelle, R.V., 2008. Origin of oxygen species in Titan's atmosphere. J. Geophys. Res. E 113, E10006.

Jurac, S., Richardson, J.D., 2005. A self-consistent model of plasma and neutrals at Saturn: Neutral cloud morphology. J. Geophys. Res. (Space Phys.) 110, A09220.

Krasnopolsky, V.A., 2009. A photochemical model of Titan's atmosphere and ionosphere. Icarus 201, 226–256.

Krivov, A.V., Banaszkiewicz, M., 2001. Unusual origin, evolution and fate of icy ejecta from Hyperion. Planet. Space Sci. 49, 1265–1279.

Landgraf, M., Liou, J.-C., Zook, H.A., Grün, E., 2002. Origins of Solar System dust beyond Jupiter. Astron. J. 123, 2857–2861.

Lara, L.M., Lellouch, E., López-Moreno, J.J., Rodrigo, R., 1996. Vertical distribution of Titan's atmospheric neutral constituents. J. Geophys. Res. E 101, 23261–23283.

Lara, L.-M., Lellouch, E., Shematovich, V., 1999. Titan's atmospheric haze: The case for HCN incorporation. Astron. Astrophys. 341, 312–317.

Lavvas, P.P., Coustenis, A., Vardavas, I.M., 2008. Coupling photochemistry with haze formation in Titan's atmosphere – Part II: Results and validation with Cassini/Huygens data. Planet. Space Sci. 56, 67–99.

Lellouch, E., Bézard, B., Moses, J.I., Davis, G.R., Drossart, P., Feuchtgruber, H., Bergin, E.A., Moreno, R., Encrenaz, T., 2002. The origin of water vapor and carbon dioxide in Jupiter's stratosphere. Icarus 159, 112–131.

Lellouch, E., Moreno, R., Paubert, G., 2005. A dual origin for Neptune's carbon monoxide? Astron. Astrophys. 430, L37–L40.

Lellouch, E. et al., 2010. Sounding of Titan's atmosphere at submillimeter wavelengths from an orbiting spacecraft. Planet. Space Sci. 58, 1724–1739.

Love, S.G., Brownlee, D.E., 1993. A direct measurement of the terrestrial mass accretion rate of cosmic dust. Science 262, 550–553.

Lutz, B.L., de Bergh, C., Owen, T., 1983. Carbon monoxide in the atmosphere of Titan: Search and discovery. Publ. Astron. Soc. Pacific 95, 593.

Lynch, R., Gamache, R.R., Neshyba, S.P., 1998. N_2 and O_2 induced halfwidths and line shifts of water vapor transitions in the (301) ← (000) and (221) ← (000) bands. J. Quant. Spectrosc. Radiat. Trans. 59, 595–613.

McKay, C.P., 1996. Elemental composition, solubility, and optical properties of Titan's organic haze. Planet. Space Sci. 44, 741–747.

Melin, H., Shemansky, D.E., Liu, X., 2009. The distribution of atomic hydrogen and oxygen in the magnetosphere of Saturn. Planet. Space Sci. 57, 1743–1753.

Moreno, R. et al., 2011. First detection of hydrogen isocyanide (HNC) in Titan's atmosphere. Astron. Astrophys. 536, L12.
Moses, J.I., Lellouch, E., Bézard, B., Gladstone, G.R., Feuchtgruber, H., Allen, M., 2000. Photochemistry of Saturn's atmosphere. II. Effects of an influx of external oxygen. Icarus 145, 166–202.
Niemann, H.B. et al., 2010. Composition of Titan's lower atmosphere and simple surface volatiles as measured by the Cassini–Huygens probe gas chromatograph mass spectrometer experiment. J. Geophys. Res. (Planets) 115, E12006.
Ollivier, J.L., Dobrijévic, M., Parisot, J.P., 2000. New photochemical model of Saturn's atmosphere. Planet. Space Sci. 48, 699–716.
Ott, S., 2010. The Herschel data processing system HIPE and pipelines up and running since the start of the mission. In: Mizumoto, Y., Morita, K.-I., Ohishi, M. (Ed.), Astronomical Data Analysis Software and Systems XIX. Astronomical Society of the Pacific Conference Series, vol. 434. ASP, pp.139–142.
Pickett, H.M., Poynter, R.L., Cohen, E.A., Delitsky, M.L., Pearson, J.C., Müller, H.S.P., 1998. Submillimeter, millimeter and microwave spectral line catalog. J. Quant. Spectrosc. Radiat. Trans. 60, 883–890.
Pilbratt, G.L. et al., 2010. Herschel Space Observatory. An ESA facility for far-infrared and submillimetre astronomy. Astron. Astrophys. 518, L1.
Poglitsch, A. et al., 2010. The Photodetector Array Camera and Spectrometer (PACS) on the Herschel Space Observatory. Astron. Astrophys. 518, L2.
Pruppacher, H.R., Klett, J.D., 1980. Microphysics of Clouds and Precipitation. D. Reidel, Mass.
Roelfsema, P.R. et al., 2012. In-orbit performance of Herschel–HIFI. Astron. Astrophys. 537, A17.
Samuelson, R.E., Hanel, R.A., Kunde, V.G., Maguire, W.C., 1981. Mean molecular weight and hydrogen abundance of Titan's atmosphere. Nature 292, 688–693.
Samuelson, R.E. et al., 1983. CO_2 on Titan. J. Geophys. Res. 88, 8709–8715.
Samuelson, R.E., Mayo, L.A., 1991. Thermal infrared properties of Titan's stratospheric aerosol. Icarus 91, 207–219.
Saur, J. et al., 2008. Evidence for temporal variability of Enceladus' gas jets: Modeling of Cassini observations. Geophys. Res. Lett. 35, L20105.
Seta, T. et al., 2008. Pressure broadening coefficients of the water vapor lines at 556.936 and 752.033 GHz. J. Quant. Spectrosc. Radiat. Trans. 109, 144–150.
Shemansky, D.E., Matheson, P., Hall, D.T., Hu, H.-Y., Tripp, T.M., 1993. Detection of the hydroxyl radical in the Saturn magnetosphere. Nature 363, 329–331.
Smith, H.T., Johnson, R.E., Perry, M.E., Mitchell, D.G., McNutt, R.L., Young, D.T., 2010. Enceladus plume variability and the neutral gas densities in Saturn's magnetosphere. J. Geophys. Res. (Space Phys.) 115, A10252.
Spencer, J.R., Howett, C.J.A., Verbiscer, A.J., Hurford, T.A., Segura, M.E., Pearl, J.C., 2011. Observations of thermal emission from the south pole of Enceladus in August 2010. In: EPSC-DPS Joint Meeting 2011, p. 1630.
Spitale, J.N., Porco, C.C., 2007. Association of the jets of Enceladus with the warmest regions on its south-polar fractures. Nature 449, 695–697.
Strobel, D.F. et al., 2010. Atmospheric structure and composition. In: Brown, R.H., Lebreton, J.-P., & Waite, J.H. (Ed.), Titan from Cassini–Huygens. Springer Science+Business Media B.V., pp. 235–257.
Tian, F., Stewart, A.I.F., Toon, O.B., Larsen, K.W., Esposito, L.W., 2007. Monte Carlo simulations of the water vapor plumes on Enceladus. Icarus 188, 154–161.
Toublanc, D., Parisot, J.P., Brillet, J., Gautier, D., Raulin, F., McKay, C.P., 1995. Photochemical modeling of Titan's atmosphere. Icarus 113, 2–26.
Vinatier, S., Bézard, B., Fouchet, T., Teanby, N.A., de Kok, R., Irwin, P.G.J., Conrath, B.J., Nixon, C.A., Romani, P.N., Flasar, F.M., Coustenis, A., 2007. Vertical abundance profiles of hydrocarbons in Titan's atmosphere at 15°S and 80°N retrieved from Cassini/CIRS spectra. Icarus 188, 120–138.
Vinatier, S., Bézard, B., Nixon, C.A., Mamoutkine, A., Carlson, R.C., Jennings, D.E., Guandique, E.A., Teanby, N.A., Bjoraker, G.L., Michael Flasar, F., Kunde, V.G., 2010. Analysis of Cassini/CIRS limb spectra of Titan acquired during the nominal mission. I. Hydrocarbons, nitriles and CO_2 vertical mixing ratio profiles. Icarus 205, 559–570.
Vuitton, V., Yelle, R.V., Cui, J., 2008. Formation and distribution of benzene on Titan. J. Geophys. Res. (Planets) 113, E05007.
Vuitton, V., Yelle, R.V., McEwan, M.J., 2007. Ion chemistry and N-containing molecules in Titan's upper atmosphere. Icarus 191, 722–742.
Wilson, E.H., Atreya, S.K., 2004. Current state of modeling the photochemistry of Titan's mutually dependent atmosphere and ionosphere. J. Geophys. Res. E 109, E06002.
Wong, A.-S., Morgan, C.G., Yung, Y.L., Owen, T., 2002. Evolution of CO on Titan. Icarus 155, 382–392.
Yung, Y.L., Allen, M., Pinto, J.P., 1984. Photochemistry of the atmosphere of Titan – Comparison between model and observations. Astrophys. J. Suppl. 55, 465–506.